Cubic -phase U–Mo alloys synthesized by splat-cooling

2013 Adv. Nat. Sci: Nanosci. Nanotechnol. 4 035006

(http://iopscience.iop.org/2043-6262/4/3/035006)

OPEN ACCESS
IOP PUBLISHING
ADVANCES IN NATURAL SCIENCES: NANOSCIENCE AND NANOTECHNOLOGY
Adv. Nat. Sci.: Nanosci. Nanotechnol. **4** (2013) 035006 (10pp)
doi:10.1088/2043-6262/4/3/035006

Cubic γ-phase U–Mo alloys synthesized by splat-cooling

Nhu-T H Kim-Ngan[1], I Tkach[2], S Mašková[2], L Havela[2], A Warren[3] and T Scott[3]

[1] Institute of Physics, Pedagogical University, 30–084 Kraków, Poland
[2] Faculty of Mathematics and Physics, Charles University, Ke Karlovu 5, 12116 Prague, Czech Republic
[3] Interface Analysis Centre, University of Bristol, Oldbury House, Bristol BS2 8BQ, UK

E-mail: tarnawsk@up.krakow.pl and tarnawsk@mag.mff.cuni.cz

Received 16 October 2012
Accepted for publication 9 May 2013
Published 14 June 2013
Online at stacks.iop.org/ANSN/4/035006

Abstract
U–Mo alloys are the most promising materials fulfilling the requirements of using low enriched uranium (LEU) fuel in research reactors. From a fundamental standpoint, it is of interest to determine the basic thermodynamic properties of the cubic γ-phase U–Mo alloys. We focus our attention on the use of Mo doping together with ultrafast cooling (with high cooling rates $\geqslant 10^6$ K s^{-1}), which helps to maintain the cubic γ-phase in U–Mo system to low temperatures and on determination of the low-temperature properties of these γ-U alloys. Using a splat cooling method it has been possible to maintain some fraction of the high-temperature γ-phase at room temperature in pure uranium. U-13 at.% Mo splat clearly exhibits the pure γ-phase structure. All the splats become superconducting with T_c in the range from 1.24 K (pure U splat) to 2.11 K (U-15 at.% Mo). The γ-phase in U–Mo alloys undergoes eutectoid decomposition to form equilibrium phases of orthorhombic α-uranium and tetragonal γ'-phase upon annealing at 500 °C, while annealing at 800 °C has stabilized the initial γ phase. The α-U easily absorbs a large amount of hydrogen (UH_3 hydride), while the cubic *bcc* phase does not absorb any detectable amount of hydrogen at pressures below 1 bar and at room temperature. At 80 bar, the U-15 at.% Mo splat becomes powder consisting of elongated particles of 1–2 mm, revealing amorphous state.

Keywords: cubic γ-U, U–Mo alloys, splat cooling, superconductivity, hydride

Classification numbers: 2.00, 4.00, 5.13

1. Introduction

1.1. Why the cubic γ-U phase?

Massive research programs in the USA were launched in the late 1970s to convert research reactors from high enriched uranium (HEU) fuel to low enriched uranium (LEU, $< 20\%$ ^{235}U) fuel.

In Vietnam, the nuclear reactor in the Central Highlands of Da Lat City had to stop working in November 2011 in order to convert HEU rods to LEU ones. It resumes activity on 20 March, 2012, equipped with 92 LEU rods for producing medical isotopes for major hospitals nationwide.

In order to develop LEU fuels, many different uranium alloys were tested. The U–Mo alloys turned out to be the most promising candidates, since they fulfill the requirements to use LEU in reactors while also preserve the cubic γ-U phase with a higher density and stability under irradiation [1, 2], e.g. they are more resistant to swelling than α-uranium based fuels [3]. U–Mo alloys were also found to be the top performers among many U-based fuel alloys in the screening-tests. More recently, U-10 wt% Mo (uranium alloying with 10% weight percent of molybdenum) was selected for the US reactors, while many European reactors continue to use the U-7 wt% Mo.

From a fundamental standpoint, it is also of interest to determine the basic thermodynamic properties of the γ-phase U–Mo alloys, since they exhibit a superconducting ground state around 2 K [4–6]. Most of the data, however, were obtained more than half a century ago. The physical and metallurgical behavior of U–Mo alloys have been reviewed up to the year 1980 [7, 8], while the phase diagram of this system up to the year 1967 has been reported [9, 10]. There is a lack of detailed and more recent data on the low-temperature electronic and magnetic properties of these γ-U alloys.

Uranium metal exhibits three allotropic phases, namely α (orthorhombic; space group *Cmcm*), β (tetragonal; $P4_2/mmm$) and γ (body-centered cubic A2-type; $Im\bar{3}m$). Until recently, electronic properties were known only for α-U stable at room temperature. Superconductivity with $T_c = 0.78$ K was reported for α-U [11–13]. β-U and γ-U phases may have different electronic properties, as their density is lower (18.06 g cm^{-3} for γ-U comparing to 19.04 g cm^{-3} for α-U). γ-U is stable only in the temperature range of 1048–1408 K [14]. The γ-U unit cell parameter (extrapolated to room temperature) is $a = 3.472$ Å [15]. In the A2 arrangement, each atom is surrounded by eight equidistant neighbors at a distance of 3.01 Å (extrapolated to room temperature) in a cubic coordination polyhedron.

1.2. How to stabilize the cubic γ-U phase?

A convenient doping can stabilize the β- and γ-phases. Typical dopants allowing U to maintain *bcc* structure down to room temperature are Ti, Zr, V, Nb, Cr, Mo, Re and Ru. Mo is recognized as being particularly efficient [16, 17] since it has a relatively large γ-phase region. At high temperatures, the U–Mo system in equilibrium has a cubic structure (γ-phase) for a solid solution in the range of 0–35 at.% Mo. Depending on the solute content and the quenching rate when U–Mo alloys are quenched from regions of γ-phase stability, combinations of α-U, β-U and γ-U and γ-like phases can occur after partial decomposition of the γ-phase. For instance cooled below 833 K, the metastable cubic γ-phase undergoes eutectoid decomposition to form the (equilibrium) orthorhombic α-phase and body centered tetragonal γ'-phase (U_2Mo intermetallics) [1]. U_2Mo (space group $I4/mmm$) is an ordered phase in the U–Mo system, which is a variant of γ phase with the atoms slightly displaced from their ideal *bcc* positions in the $(001)_\gamma$ directions (the tetragonal *c*-axis) which arrange themselves in a closer spacing than the γ-phase [18]. The unit cell parameters of U_2Mo are: $a = 3.427$ Å, $c = 9.834$ Å; $c/a = 2.86$). The so-called γ°-phase [18–20] can be also formed in quenched U–Mo alloys. Such a phase was considered as a normal tetragonal structure with a small contraction of the original *c*-axis of the *bcc* cell, i.e. with lattice parameters $a(\gamma^\circ) = a(\gamma)$ and $c(\gamma^\circ)$ slightly less than $c(\gamma)$ and the ratio c/a being very close to 1.0 [19]. However, other authors considered the tetragonal γ° cell to be related to the *bcc* cell by doubling a and contracting the original *c*-parameter, i.e. $a(\gamma^\circ) \sim 2 \bullet a(\gamma)$ and $c(\gamma^\circ)$ slightly less than $c(\gamma)$ and the ratio c/a very close to 0.5 (i.e. $2 \times 2 \times 1$ *bcc* cell) [18, 20]. The important issue is that by choosing a proper combination of Mo content and cooling rate (from the high-temperature solid solution to room temperature) the metastable γ-phase can be retained at room temperature. For a review of the minimum required molybdenum concentration to ensure a single-phase γ-alloy and the related sample-treatment conditions (cooling temperature and media) see the introduction in [21]. For instance under normal furnace cooling conditions (as-cast), the single-phase γ-alloy has been reported for U–Mo alloy with 16.5 at.% Mo (8 wt% Mo) [1], while under ultrafast cooling (from the melting temperature to room temperature), the single-phase γ-U was stabilized by alloying with 15 at.% Mo [21]. Using centrifugal atomization method, the atomized powder of a single-phase γ-U alloy was reported for U-4 at.% Mo alloy (2 wt% Mo) [22].

1.3. The use of ultrafast cooling in stabilizing the cubic γ-U phase

We focus our attention on the use of Mo doping together with ultrafast cooling (splat-cooling technique), which helps to maintain to some extent a high-temperature state to room temperature and below it. Rapid quenching (with high cooling rates $\sim 10^6$ K s^{-1}) of certain alloys from the melt could form extended solid solutions, new metastable crystalline phases and amorphous solid phases [23]. Splat cooled uranium has been used since the 1960s in the course of the search for novel microstructures, coming into focus more recently as a source of glassy or amorphous uranium [24] for superconductor and electromagnetic experiments. Aside from cursory optical metallographic study in the early 1960s [25] and study of modification of uranium magnetism and/or superconductivity in the splat-cooled uranium metal and alloys [26, 27] as compared with their crystalline counterparts, no detailed metallurgical characterization work has been conducted.

Our goal is to prepare a single-phase *bcc* material in U–Mo system (stable or metastable) and to determine low-temperature properties of these γ-U alloys. In our first attempt of characterization of the as-formed U–Mo alloys without any additional sample treatment, the 100% pure cubic γ-U phase was observed in U–Mo alloy with 15 at.% Mo [21]. The most significant finding of our study has been the demonstration that using a splat cooling method it has been possible to maintain some fraction of the high-temperature γ-phase at room temperature in pure uranium, something which was hitherto considered impossible. In the second step of our study we examine the stabilization of the cubic phase. In this work we describe the phase transformation/decomposition and/or stabilization of the γ-uranium phase in U–Mo alloys upon ageing, annealing at 500 and 800 °C for annealing time of 1–144 h as well as upon hydrogenation. For a comparison, the results obtained for a splat-cooled pure-U specimen are also presented.

2. Experimental

U–Mo alloys examined in this study were cast using high-purity natural U (2N8 or better) and Mo (3N8) by means of arc-melting of nominal U–Mo concentrations with 0–17 at.% Mo. In many publications, the notation U–*X*Mo is often used, where *X* stands for the Mo amount given in a weight percentage (wt%), e.g. alloy with

10 wt% molybdenum referred to as U–10Mo. In our case, the Mo concentration is given in the atomic percentage (at.%). In order to avoid a possible mistake, we use the following notation: U–Mo*X*, e.g. alloy with 10 at.% molybdenum $U_{0.90}Mo_{0.10}$ (approximate 4.5 wt% Mo) referred to as U–Mo10. The mass of each alloy piece was between 200 and 400 mg, so as to be suitable for subsequent splat cooling. To ensure homogeneity of the alloys, the sample buttons were turned over and re-melted three times. Each sample was subsequently transferred to a splat cooling system (high-vacuum splat-cooler by Vakuum Praha). The material loaded into this splat-cooling system is again arc-melted and the molten drop falls between two Cu pistons, triggering a photoelectric switch that initiates piston activation and entraps the falling drop between the two piston heads. This process is assumed to yield a typical cooling rate in the order of 10^6 K s^{-1} and results in irregularly shaped disc of splat-cooled material of approximately 20 mm diameter and 100–150 μm thickness. The mass loss of the sample after arc-melting is about 0.1% and after splat-cooling is almost zero. Therefore, the sample compositions were assumed to correspond to the nominal ones.

For each U–Mo alloy, we have prepared several splats. One set was kept in air and checked regularly by x-ray diffraction (XRD) after 1, 3, 6 and 12 months. Two sets of U–Mo samples were used for different annealing runs, at 500 °C (773 K) and 800 °C (1073 K), each for 1, 4, 10, 72, and 144 h, i.e. at two different temperature values, the lower one in the range for eutectoid decomposition of γ-phase to form the equilibrium α-phase and U_2Mo intermetallic compound (γ'-phase), and the higher one within the temperature range of stability of γ-phase U–Mo alloys. Sinha *et al* [1] reported that annealing of single γ-phase U–Mo alloys (e.g. with 16.5 at.% Mo) at 500 °C for 68 h already led to a formation of mixed phase (orthorhombic α-phase, U_2Mo intermetallic and the cubic γ-phase). Thus, subsequent annealing with shorter time was chosen (e.g. 1, 4 and 10 h) so that we could follow the development of various phases in these alloys. The annealing was performed in sealed quartz tubes with Ar atmosphere. At the end, the tubes were removed from the furnace and left at ambient temperature to cool down for 10–20 min.

The hydrogenation was performed by exposure the U–Mo splat-cooled alloys to H_2 gas. The sample could be loaded in the hydrogenation equipment which works with a maximal pressure applied of 160 bar and with a thermal treatment up to 773 K.

The crystal structure of the U–Mo splats were characterized by XRD using a Bruker D8 Advance diffractometer with Cu-K_α radiation. Data was collected with a 2θ-step of 0.02° in a 2θ-range of 20–130° and a counting time of between 8 and 12 s per step. We have checked both the as-formed samples (with non-treated surface) as well as scraped/polished splat surface.

For other measurements, the sample-pieces cut by spark erosion were used, e.g. rectangular-shaped pieces of approximately 1×3–4 and 2×2 mm^2 were, respectively, used for the electrical resistivity and specific-heat measurements. The resistivity measurements were carried out in a standard four-probe configuration using a CCR system (in the temperature range 3–300 K and in zero applied field) and by means of PPMS (quantum design physical properties measurement system) in applied magnetic fields (0.3–4.2 K, magnetic fields 0–5 T). The specific-heat measurements were performed by using PPMS (0.3–300 K).

The microstructure of the splat U–Mo alloys were studied by electron back-scattering diffraction (EBSD) and a focused ion beam (FIB). Several spark-cut pieces from different parts of different splats were examined to ensure the reproducibility of the obtained results. The microscope used for EBSD analysis was a Zeiss EVO MA10 fitted with LaB_6 electron source and a Digiview 3 high-speed camera with associated EBSD instrumentation from EDAX. Diffraction data was recorded and processed using OIM™ software. The FIB instrument (FEI FIB-201 model) was used. More details of sample preparation and treatment for EBSD and FIB analysis were reported elsewhere [21].

3. Results and discussion

3.1. The as-formed U–Mo splats

The XRD patterns of the splat-cooled U–Mo alloys in the as-formed state are shown in figure 1. For an easier comparison, we show the normalized XRD pattern (i.e. the intensity of the most intense reflection at around 36° ($= 2\theta$) was set to 1). They are then shifted upwards along the *y*-axis with respect to each other to guide the eyes. Phase analyses using XRD are summarized as follows:

1. The double-phase ($\alpha + \gamma$) structure was obtained in the splat-cooled U–Mo alloys with Mo content $\leqslant$ 10 at.%. We notice here that EBSD revealed a small amount of the (cubic) γ-U phase retained at room temperature alongside the majority (orthorhombic) α-U phase even if in the splat-cooled pure uranium specimens (0 at.% Mo). XRD pattern of the pure U splat has revealed all expected α-U peaks and some additional reflections attributed to γ-U. The intensity of reflection of α-U largely decreases with increasing Mo content, while the reflections of γ-U increase visibly. Moreover, all the γ-reflections appear as single and sharp peaks except for the diffuse reflection at 35.8° (the overlapped $\alpha(021) + \gamma(110)$ peak). We notice here that well separated $\alpha(021)$ and $\gamma(110)$ peaks were observed for water-quenched $U_{0.94}Mo_{0.06}$ alloy (6 at.% Mo) [28]. The appearance of the γ phase in U–Mo alloys with Mo content $\leqslant$ 10% is not very surprising, since the double ($\alpha + \gamma$) phase was already found to exist in U–Mo alloys with 3.3–3.5 at.% Mo [29, 30].
2. For all alloys with $\geqslant$ 11 at.% Mo, the recorded diffraction peaks can be attributed exclusively to γ-type reflections, i.e. without any (orthorhombic) α-phase. In particular the intense peak at 35.8° became narrower, indicating that it contains mostly the $\gamma(110)$ reflection.
3. For U–Mo11 and U–Mo12, a splitting of the γ reflection into a doublet with unequal intensity was observed for all γ-peaks (see figure 1(b)), indicating that these alloys have actually the designated γ°-phase [19].
4. Single-peak character was observed in U–Mo12.5 for all high-angle γ-reflections. Although no visible splitting of the $\gamma(110)$ reflection was observed, a trace of doublet-type was still present (figure 1(b)) revealing that

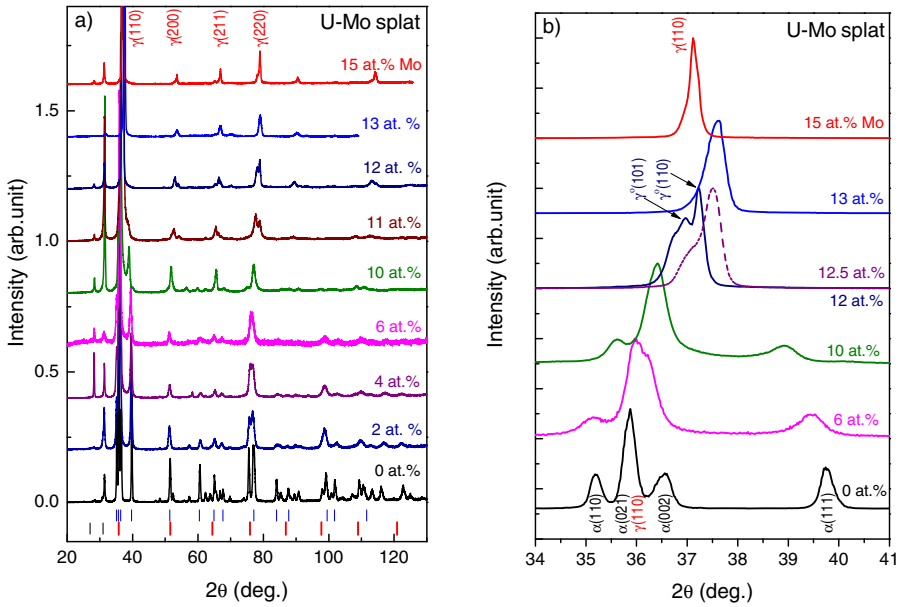

Figure 1. (a) X-ray diffraction pattern of as-formed U–Mo alloys prepared by splat cooling. Each curve was normalized to the maximal intensity of the most intense peak at $2\theta = 36°$–$37°$ and then shifted upwards with respect to that of pure U-splat (0 at.% Mo). The (color) vertical sticks indicate the main XRD patterns of orthorhombic (blue) and cubic (red) structures and of the surface impurities (black). The four main γ-reflections are also indicated. (b) The low-angle x-ray reflections of selected U–Mo alloys revealed a phase transformation from the double $(\alpha + \gamma)$ phase for alloys with 1–10 at.% Mo to γ° phase for alloys with 11–12.5 at.% Mo (splitting of the γ-reflections into doublets) and pure cubic γ phase for alloys with $\geqslant$ 13 at.%Mo (single γ-reflections).

the $\gamma^\circ \rightarrow \gamma$ transformation in this alloy was still not complete.

5. The XRD pattern revealing single sharp γ-peaks characterized for 100% pure cubic γ-phase was obtained for U–Mo13 and U–Mo15. Although the observed γ-peaks for U–Mo13 are not as sharp as those for U–Mo15, however, they are not split (i.e. all are single peaks).
6. The additional peak observed at $2\theta = 65.2°$ was attributed to $U_2Mo(213)$ in our first report [21], although we did not exclude the contribution of UC(222), since these peaks are very close to each other. However, detailed investigations of the U–Mo alloys with γ-structure revealed some correlation between the developments of such a peak with increasing Mo content. The relative intensity of UC(111) peak did not change much with changing the Mo content, indicating a similar contamination in these alloys. Thus if such a peak $2\theta = 65.2°$ was originated from carbon contamination (UC(222) suspected), it would not show any dependence on the Mo content. Instead, we observed that its relative intensity increases with increasing Mo content. Besides, it became more and more separated from the $\gamma(110)$ one. The results confirmed that this peak is originated (only) from $U_2Mo(213)$. For the U–Mo12 alloy, an overlapping of these peaks was observed, as they were close to each other ($U_2Mo(213)$ reflection located at 65.2° and the $\gamma(110)$ one at 66.4°). The $\gamma(110)$ reflection shifted upwards to higher angles with increasing Mo content, e.g. in the alloy with 17 at.% Mo it located at 66.9° providing a good separation between these two peaks.
7. The calculated lattice parameters (a, b, c) determined for the γ°/γ phase detected in the splat-cooled U–Mo alloys [21], especially the values for the c/a ratio for the γ°-phase alloys (0.98–0.99), are in good agreement with those reported earlier [29]. At low angles, peaks corresponding to UO_2 and UC were observed irrespective of composition, originating mostly from the surface of the splats (as they are suppressed by scraping/polishing).

For a clear view of the phase development in splat-cooled U–Mo alloys, the low-angle XRD patterns of selected U–Mo alloys are shown in figure 1(b). The XRD patterns obtained for samples with 0–10 at.% Mo are very similar, except for the fact that with Mo doping ($\geqslant$ 1 at.%) the $\alpha(002)$ peak was merged to the overlapped $\alpha(021) + \gamma(110)$ peak forming a very diffuse peak at 36°. With increasing Mo concentration the intensity of α-U peaks largely decreases. Besides, whilst alloys with Mo concentration up to 6 at.% exhibited almost no shift of the α-peaks, a significant shift of these peaks was observed with further increasing of the Mo concentration up to 10 at.%. This was ascribed to a large contraction in the b-parameter of the regular orthorhombic structure, resulting in what is traditionally referred to as the α'_b-phase [19]. In other words, these intermediate Mo-concentrations (6–10 at.% Mo) consisted of the mixed $(\alpha'_b + \gamma)$ phase. As we mentioned above, for U–Mo11 and U–Mo12, the splitting of the γ-reflection into a doublet was observed for all γ-peaks. As an example, it is shown in figure 1(b) that the $\gamma(110)$ reflection of U–Mo12 splits into a doublet located around 37.0° ($\gamma^\circ(101)$) and 37.2° ($\gamma^\circ(110)$). In U–Mo12.5, although the $\gamma^\circ(101)$ reflection disappeared, a shoulder-like feature was observed indicating that such an alloy still consists of a mixed $\gamma^\circ + \gamma$(dominant) phase. Increasing Mo content to 13 at.%, all γ-reflections exhibit as single-type peaks, e.g. the $\gamma(110)$ reflection at 37.6°, revealing that it consists of 100% pure cubic γ-phase. However, all these peaks are diffuse, considered to be corresponding to 'superlattice' reflections caused by the atom shifts (from their ideal A2

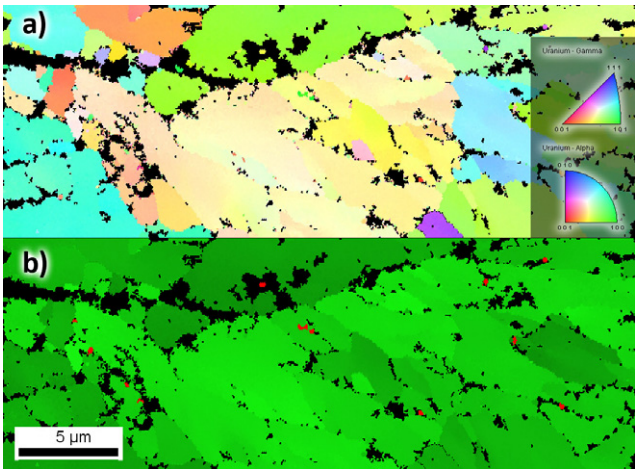

Figure 2. EBSD maps recorded from the pure uranium splat surface showing (a) crystallographic orientation and (b) phase distribution. The metal is predominantly α-U (green) with small and well dispersed γ-U (red) grains. (These EBSD maps exhibiting some fraction of the γ-U phase persisting at room temperature in pure uranium were chosen as the logo for the AVS 59 Call for Actinides and Rare Earth Abstracts, 28 October–2 November, 2012, Tampa, Florida, USA).

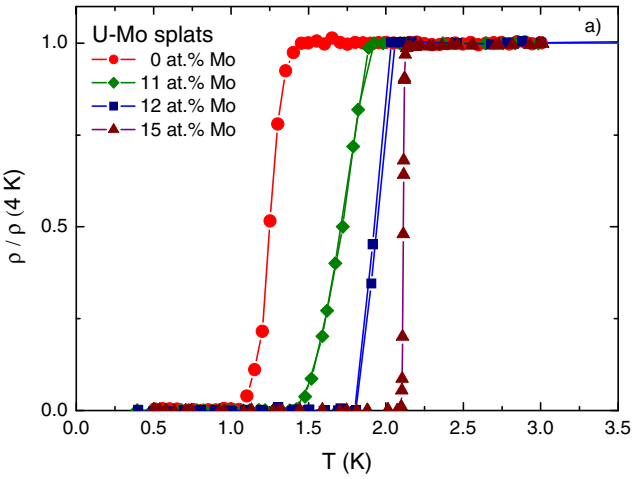

Figure 3. The superconducting phase transition of selected splat-cooled U–Mo alloys revealed by a single jump in the electrical resistivity curve.

sites). Increasing the Mo concentration to 15 at.%, the γ-peaks become very sharp, e.g. the $\gamma(110)$ reflection located at 37.1°, revealing that they are corresponding to the fundamental A2 structure reflections. Moreover, all those sharp peaks are shifted to lower reflection angles, indicating a small unit cell contraction of the ideal cubic γ-phase where the atoms locate at their A2 structure sites (i.e. no atom displacements from their ideal *bcc* sites) in U–Mo15 alloy.

EBSD analysis was so far performed on the pure uranium and U–Mo15 alloy. For both splat samples, crystallographic and phase mapping were performed on surface and sectional cuts through the alloy. The EBSD maps recorded from the cross-sections revealed an unusual microstructure of the splat-cooled pure uranium, which exhibits a range of distorted grains shapes and intra-granular twinning. Grain sizes were typically large, with the modal average being 24.6 μm diameter, and exhibited a preference for a (101) orientation. A significant number of twins were observed. The most abundant were narrow 69° misorientations ({130} twins), although there were a number of much wider 90° misorientations ({172} twins) [21]. No γ-phase was detected with any confidence throughout the cross-section, only α-U was recognized. Despite the distorted structure observed throughout the splat, no evidence for dendritic growth was observed, unlike many other splat cooled metals. For the U–Mo15 alloy, the data clearly indicated the presence of a γ-U phase structure with no detectable α-U. The EBSD crystallographic and phase mapping of the ion-sputtered regions of the surface of the pure uranium splat is shown in figure 2. It indicates with good confidence a predominantly α-U structure with rare, isolated grains of γ-U typically no more than 1 μm in maximum dimension. As the surface of the splat would be subject to the most rapid cooling, it is also the region where the γ-phase is most likely to be preserved compared to the bulk of the sample. The γ-phase observed using EBSD were both intra-granular micrograins (typically sitting along sub-boundaries) and inter-granular micrograins. Although the EBSD confirmed the XRD results for the existence of γ-phase, the scarcity of grains in the EBSD images does not correlate well with the intensity of the peak in the XRD data. We assume that the electropolishing used to prepare the sample for EBSD has removed a sizable volume of the surface and thus it is possible that quantities of γ-phase (mostly concentrated on the surface) were removed at that point. The EBSD maps recorded that the surface microstructure of splat-cooled U–Mo15 alloy has revealed an equigranular grain structure, not crystal twinning and no obvious preferred crystallographic orientation. EBSD mapping identified only γ-U phase, with no evidence for α or α-related phases, but some isolated monocarbide (UC) inclusion particles [21]. The crystal structure appears to be finer than that of the pure uranium splat (modal average diameter of 3.1 μm, with over 60% of grains between 3.1 and 5.2 μm), and shows fewer signs of distortion. We notice here that one EBSD map indicated that there was a possibility of grain size varying significantly across a cross-section of the sample.

Additional tools to distinguish between the various U phases are low-temperature measurements of electrical resistivity and specific heat. They bring information on superconductivity (interesting also by itself), as superconducting properties differ in individual phases.

No significant anomaly related to the charge-density-wave (CDW) transitions [11–13] in the temperature range of 20-50 K was revealed, either for the splat-cooled uranium specimen or for its bulk precursor [21]. The resistivity values of the splat-cooled samples at room temperature increase with increasing Mo content generally attributed to the atomic disorder. A rapid flattening of $\rho(T)$ curves with increasing Mo concentration was observed amounting even into a negative resistivity slope ($d\rho/dT < 0$) for alloys with $\geqslant 11$ at.%Mo. The U–Mo splats become superconducting with T_c ranging from 1.24 K (for pure-U specimen) to 2.11 K (for U–Mo15). Only one sharp resistivity jump at the transition was observed, as shown in figure 3. The temperature dependence of the critical field $H_{c2}(T)$ for the U–Mo alloys [21] revealed neither a quadratic dependence as the temperature approaches 0 K expected for classical

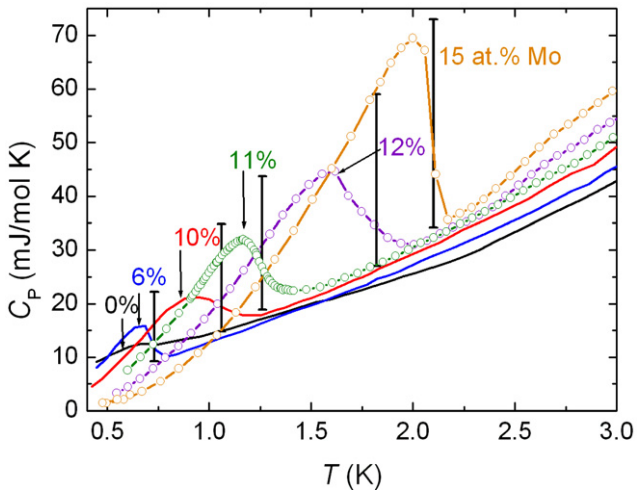

Figure 4. Superconducting phase transition in U–Mo splats revealed in the specific heat. The vertical bars indicate the theoretical BCS values $1.43^{*}\gamma_e^{*}T_c$ (see text).

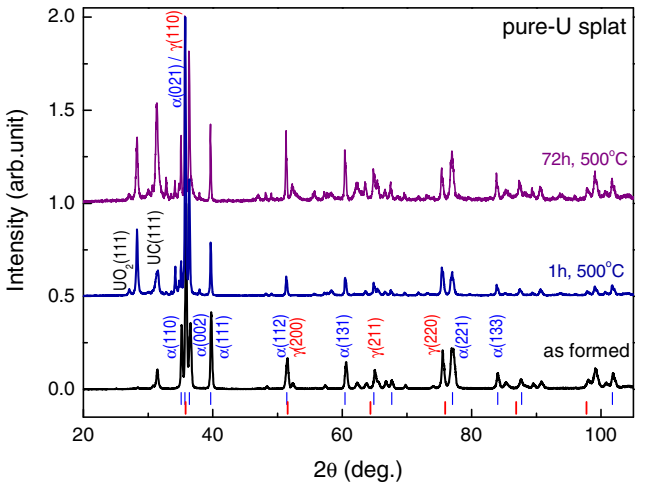

Figure 5. Comparison of XRD pattern of the pure-U splat in the as-formed state with those upon annealing at 500 °C for different times. (The curves were normalized and shifted for clarity). The (color) vertical sticks indicate the main peak positions for the (blue) orthorhombic and (red) cubic structures. The four main cubic γ-phase reflections are also labeled.

low-T_c superconductors with orbital limiting, nor a close to linear dependence typically exhibited by strongly interacting Fermi liquid superconductors as e.g. U_6Fe [31]. It is therefore difficult to estimate the limit ($T \geqslant 0$) value $H_{c2}(0)$. Applying tentatively the Werthamer–Helfand–Hohenberg theory for a weakly coupled superconductor in a clean limit [32], we obtain $\mu_0 H_{c2}(0) = 5.3$ T for U–Mo15. Taking into account the deviation from the quadratic dependence mentioned above, the actual $\mu_0 H_{c2}(0)$ can be somewhat higher.

The Sommerfeld coefficient of electronic specific heat γ_e and the Debye temperature were estimated from the normal state from a linear fit of C_p/T versus T^2 in the T^2-range between 4 and 100 K^2. It yields the value $\gamma_e = 9.1$ mJ mol^{-1} K^{-2} for the bulk uranium, which is in good agreement with that reported for α-U single crystal (9.13 mJ mol^{-1} K^{-2}) but lower than that for polycrystalline samples [12]. For the pure U-splat, γ_e was estimated to be 11 mJ mol^{-1} K^{-2}. The moderate increase of the Sommerfeld coefficient γ_e is emphasized when normalizing to mole of uranium 16 mJ mol^{-1} K^{-2} for 15 at.% Mo corresponding to uranium 18.8 mJ mol^{-1} K^{-2}, i.e. the value doubled comparing to α-U.

We try to deduce some parameters from a combined analysis of our specific-heat and resistivity results. Using the quadratic coefficient of resistivity a and the electronic specific-heat coefficient γ_e (see equations (1) and (2) in [21]), the a/γ_e^2 ratio was estimated to be $1.1 \cdot 10^{-5}$ and $1.3 \cdot 10^{-5}$ $\mu\Omega$ cm K^{-2} (mJ mol^{-1} K^{-2})^2, respectively, for the bulk and splat-cooled uranium. These values are not very different from approximate value of 1×10^{-5} expected from the Kadowaki–Woods relation. That means that the coefficient a indeed reflects the electron–electron scattering.

The specific heat of splat-cooled U–Mo alloys down to 0.4 K are presented in figure 4. The superconducting transition shows up as a λ-type peak in the specific heat $C(T)$. While all other samples revealed only a single peak on the $C(T)$ curves, a double peak feature was observed for U–Mo11. We tentatively attribute this finding to a coexistence of γ and γ° phase. The most pronounced λ-type anomaly was found for U–Mo15. The height of the jump ΔC exceeds somewhat the value expected from the BCS theory, $\Delta C = 1.43^{*}\gamma_e^{*}T_c$ (where γ_e is the normal-state Sommerfeld coefficient of electronic specific heat), marked in figure 4 by a vertical segment.

3.2. Stability of U-splats against ageing and annealing

The XRD measurements were performed on the splat-cooled pure U specimen kept in atmospheric conditions after 1, 3, 6 and 12 months. Except for a small change in the relative peak-intensity, no visible change was observed. In particular, all the γ-peaks are well preserved. Our results thus indicate that both α- and γ-phase formed in the splat-cooled U-specimen have a long-term stability at ambient conditions.

No change in the XRD patterns of the pure U-splat was revealed upon annealing at 500 °C up to annealing time of 144 h, except for some small changes in the relative peak intensity. Figure 5 shows the comparison of XRD pattern of the pure-U splat in the as-formed state with those upon annealing at 500 °C for various annealing times. Each curve was normalized to the maximal intensity of the most intense peak at $2\theta = 36^{\circ} - 37^{\circ}$. The curves were then shifted for clarity. Figure 5 also contains the vertical sticks at the bottom indicating the main XRD lines of the orthorhombic and cubic structures. Increasing annealing time mostly implies a larger sample contamination showed by a large increase of the peak-intensity related to oxides and carbides. Moreover, the background signal increases enormously after 72 h. Increasing annealing time to 144 h leads to a strong increase of the UC (111) peak and an appearance of high-angle UC/UO_2 peaks.

3.3. Phase transformation versus phase stabilization in U–Mo splats

Similar to pure U-specimen, all U–Mo alloys are very stable when exposed to atmospheric conditions, no visible change in XRD pattern was observed after e.g. 1 year.

Figure 6 shows a comparison of XRD pattern of the splat-cooled U–Mo12 alloy in the as-formed state with those

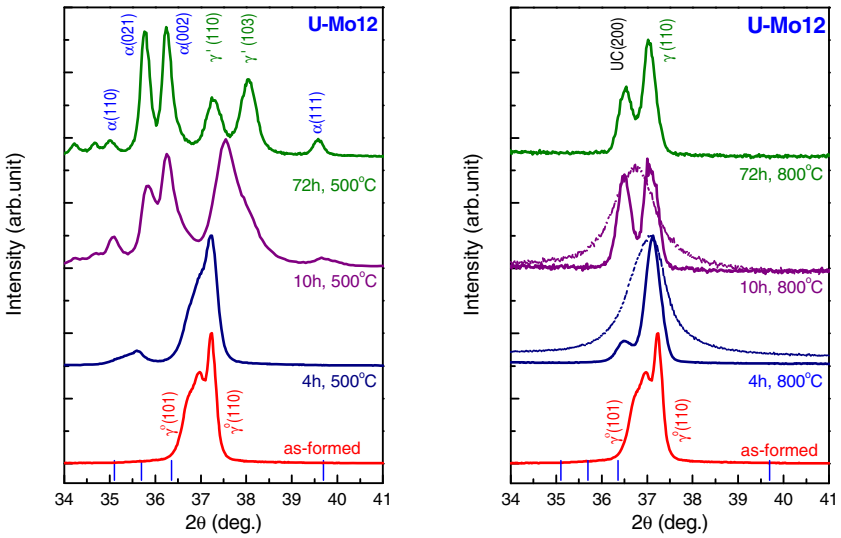

Figure 6. Comparison of (low-angle) XRD pattern of the U-12 at.% Mo splat in the as-formed state (γ°-phase) with those upon annealing at 500 °C (left) and 800 °C (right) for different annealing time. The (blue) vertical sticks indicate the main reflections of the orthorhombic structures. Solid lines show the results obtained on samples just after annealing, while those after sample scraping to remove partially surface contaminations (e.g. carbide) are indicated by dashed lines.

upon annealing at 500 and 800 °C for various annealing times. Upon annealing at 500 °C (773 K), the $\alpha(021)$ reflection appeared after annealing for 4 h (figure 6, left). With further increasing annealing time (10 h), more and more α-U reflections appeared. Besides, they are gradually more intense. After 72 h, the two main α-reflections, $\alpha(021)$ and $\alpha(002)$, are well separated from each other and have almost equal intensity. The double γ peak around 37° ($\gamma^\circ(110)$ and $\gamma^\circ(101)$ peak of the γ°-phase) merged into one broad and asymmetric peak upon annealing after 4 h, which then becomes more symmetric and shifted toward higher angles after 10 h. Upon further annealing such a peak was split into two separated peaks assigned as $\gamma'(110)$ and $\gamma'(103)$ reflection of U_2Mo intermetallics. Moreover, high-angle γ' peaks were observed (at 53.6°, 55.8°, 79.2°, 81.2°, respectively for $\gamma'(220)$, $\gamma'(213)$, $\gamma'(200)$, $\gamma'(206)$). The results confirmed that annealing at $T = 773$ K leads to a decomposition of the initial γ°-phase and γ°–γ' transformation, yielding a composite ($\alpha + \gamma'$) structure in U–Mo12 alloy. We can compare with literature [30] reporting that the appearance of the α-phase lines not until 3 h annealing (at the same temperature 500 °C) was observed for U–Mo9 alloy which had undergone additional sample treatments and exhibited the pure γ phase in the as-obtained state. We notice here that the α-reflections are located at the expected reflection angles of the α-U phase, indicating that the α-phase formed due to the γ decomposition does not show any significant change in the lattice parameters. A small but visible peak-shift to higher reflection angles, however, was observed for the $\gamma^\circ \rightarrow \gamma'$ transformation, indicating that such a process implies a certain decrease in the lattice parameters which can be an indication of an increase of the Mo content in the γ' phase [30]. No peaks associated with the decomposition of the γ°-phase were found upon annealing at 800 °C (1073 K) for different annealing times up to 144 h (figure 6, right). The double γ°-peak (i.e. $\gamma^\circ(101)$ and $\gamma^\circ(110)$ located, respectively, at 36.9° and 37.2° in the as-formed state) has changed into a single broad(er) peak located at 37.2° after annealing of 1 h. Increasing the annealing time to 4 h implies an appearance of a satellite peak at 36.5°. Such a peak became much enhanced with increasing annealing time. We notice here that, unlike annealing at 500 °C, no peak shift and no peak-splitting was observed for all γ-reflections upon annealing at 800 °C up to 72 h, e.g. the $\gamma(110)$ reflection is always located at around 37.2°. Besides, no peak appeared at 37.9°, i.e. at expected position of the $\gamma'(103)$ reflection. Thus, we assumed that annealing at 800 °C leads to the $\gamma^\circ \rightarrow \gamma$ transformation and stabilization of such γ phase, which does not have to be accompanied by change in the lattice (or any change in the Mo concentration). The additional peak at 36.5° has a contribution of UC(200) from the surface contamination. It is visible that increasing annealing time leads to an appearance of more and more UC as well as UO_2 reflections with a higher intensity. Obviously, increasing annealing time would lead to more surface contamination. In order to confirm it, we have performed the XRD also on the annealed sample after scraping the surface (i.e. removing the surface contamination). The comparison of data obtained on annealed samples at 800 °C before and after scraping is presented in figure 6, right. The scraping produces a large reduction of UC peaks. For instance the (relative) intensity of UC(111) reduced by 50% after scraping. As is shown, a large reduction of the peak at 36.5° was observed confirming that it is originated from UC(200). The scraping can also influence the microstructure of the splat surface, as evidenced by a large broadening of the $\gamma(110)$ peak. We notice here that upon annealing at 500 °C, no visible UC(200) was observed. Such a peak is very close to that of $\alpha(002)$. The intensity of $\alpha(200)$ reflection is much enhanced in this case. Namely, for the as-formed splats with mixed phases, the $\alpha(021)$ reflection (at 35.4°) was the most intense one, while for the splats consisting of α-phase from the γ-decomposition, the peak at around 36.5° turned out to be the most intense one. We assumed that such a peak was as a result of overlapping of the $\alpha(002)$ and UC(200) ones (at 36.4° and 36.5°, respectively).

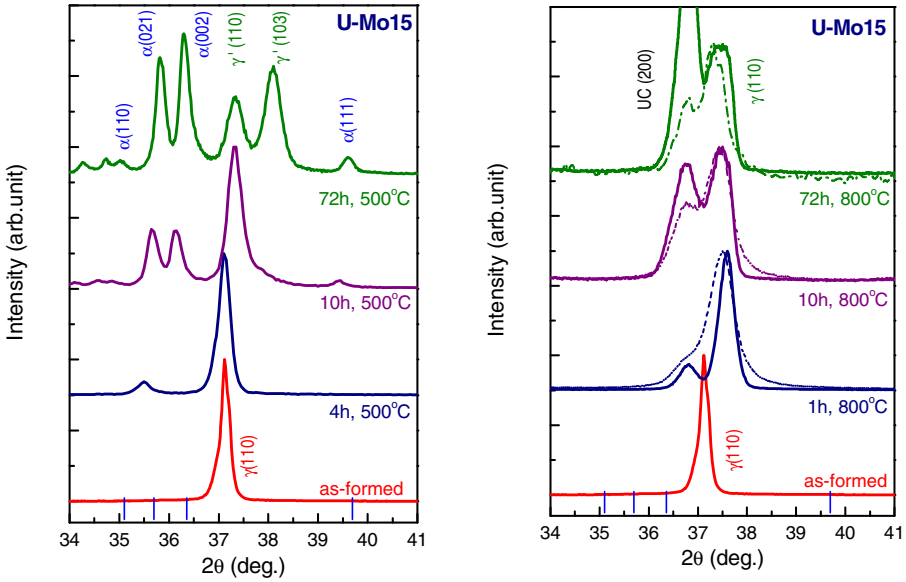

Figure 7. Comparison of (low-angle) XRD pattern of the U-15 at.% Mo splat (U–Mo15) in the as-formed state (pure cubic γ-phase) with those upon annealing at 500 °C (left) and 800 °C (right) for different annealing time. The (blue) vertical sticks indicate the main reflections of the orthorhombic structures. Solid lines show the results obtained on samples just after annealing, while those after sample scraping to remove partially surface contaminations (e.g. carbide) are indicated by dashed lines.

A similar change was observed for U–Mo15 upon annealing at 500 °C (773 K), shown in figure 7 (left). Namely, annealing leads to a partial decomposition of the γ-phase to form the equilibrium α-phase and the intermetallic compound U_2Mo (revealed by the appearance of the γ' (110) and γ' (103) reflections). The pure cubic γ-phase in the as-formed state shows up as sharp γ peaks. Annealing at 500 °C only leads to a small broadening of the γ reflections. Similar to U–Mo12 alloy, a shift toward higher angles was also observed in this case, indicating a small change in the lattice parameter related to $\gamma \rightarrow \gamma'$ phase transformation. During the ordering process the larger uranium atoms become closer together. The smaller molybdenum atoms after ordering are surrounded by atoms at a slightly greater distance than in the disordered state. The γ-phase was well stabilized upon annealing at 800 °C, as shown in figure 7, right. The $\gamma(110)$ peak was shifted visibly towards the higher angles after annealing of 4 h. No further peak-shift was observed with increasing annealing time ($\geqslant$ 10 h). However, a large peak-broadening of e.g. $\gamma(110)$ was revealed. The peak broadening for U–Mo15 alloy is even more enhanced than that for U–Mo12 alloy. It indicates that the cubic phase has very inhomogeneous molybdenum distribution. The additional peak at around 36.5° was attributed to UC(200) due to its specific behavior (e.g. its intensity was much enhanced with increasing annealing time and it was much suppressed after scraping the sample surface). More peaks attributed to UC and UO_2 were observed at high angles for long annealing time, revealing more surface contamination upon annealing at 800 °C (in comparison with that at 500 °C). In this case, annealing at 800 °C leads to a stability of the cubic γ-phase without $\gamma \rightarrow \gamma'$ (disordered-ordered) phase transformation. Not only the $\gamma(110)$ peak but all other γ-peaks are diffuse, indicating a Mo inhomogeneity in the sample.

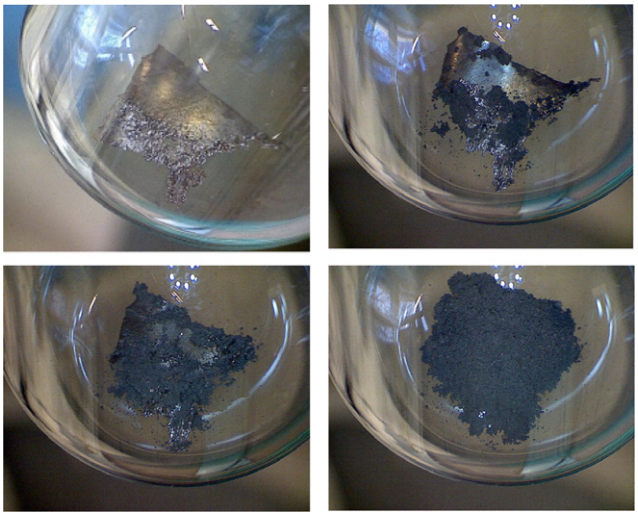

Figure 8. Photographs of pure U splat during hydrogenation process at 1 bar and at room temperature (in a glass reactor) showing a gradual change of the metallic-luster piece of a splat into dark fine powder of the hydride UH_3.

3.2. Hydrogenation

H absorption at room temperature was tested for pure-U splat and γ-phase UMo15 alloy. The α-U readily absorbs hydrogen even at room temperature forming UH_3. The piece of a splat uranium specimen, which had a metallic luster, has gradually turned into dark fine powder upon hydrogenation, as shown in figure 8. Unlike α-U, the cubic *bcc* phase does not absorb any detectable amount of hydrogen at pressures below 1 bar and at room temperature even on timescale of days. Upon applying high pressure of H (80 bar), the metallic luster piece of U–Mo15 splat has turned into dark elongated brittle particles 1–2 mm long, shown in figure 9, clearly indicating the formation of a hydride of the γ-U alloy. (We cannot use the glass reactor at high pressures

Figure 9. Photograph of U-Mo15 alloy after hydrogenation at 80 bar. The hydride consists of elongated particles 1–2 mm long displayed on a background of a millimeter grid.

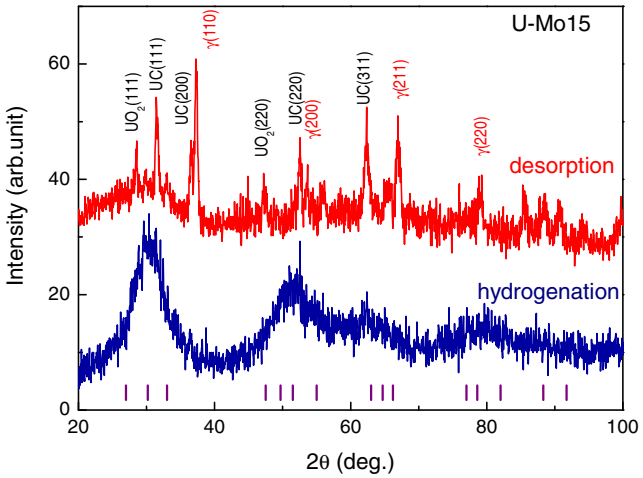

Figure 10. XRD pattern of U–Mo15 hydride formed at hydrogen gas pressure of 80 bar before and after desorption. The vertical sticks indicate the peak positions for β-UH_3.

and thus photos cannot be taken during the hydrogenation process.)

To quantify the amount of absorbed hydrogen, the U–Mo15 hydride was decomposed in a closed evacuated volume by heating up to 800 °C. In the first stage the temperature is ramped up using the rate 4 °C min^{-1}. It is seen that the H release took place in two stages. The first stage around $T = 200$ °C is followed by a more massive one around 350 °C. After this stage is completed (around 400 °C) the H pressure does not increase any more. The released gas producing the pressure of 155 mbar in the reactor was not evacuated after the furnace was switched off. The cooling led to a re-absorption of the part of the gas. As the total amount of the released H corresponds to approx. 3.0 H/U atom, we suspected therefore that the procedure leads to the formation of UH_3. The XRD pattern, as shown in figure 10, does not prove that. Instead it points to amorphization, exhibiting several broad features only. In general, hydrogenation-induced amorphization is not uncommon (see e.g. [33]). It can be attributed to a situation, in which the local atomic arrangement minimizing the energy is not compatible with a long-range crystal periodicity, preferring a short-range atomic order.

The fact that powder U–Mo alloy can be obtained by this method can have a technological significance.

4. Conclusions

The current work with ultrafast cooled U–Mo alloys has demonstrated the stabilization of the γ°-phase and pure cubic γ-phase in uranium alloys containing 11-12 and 13-17 at.% Mo, respectively, in the as-formed state without any additional sample-treatment and without reversion to an α-phase. These phases are very stable when exposing to ambient conditions.

Our investigations show also that by ultrafast cooling at cooling rates of $\sim 10^6$ K s^{-1}, it has been possible to preserve a small amount of the high-temperature cubic γ-phase at room temperature in pure uranium. Besides, it reduces the necessary concentration of Mo as a stabilizing dopant. This opens a new possibility of stabilizing the γ-phase at room temperature in uranium alloys by ultrafast cooling.

The U–Mo splats also become superconducting with T_c ranging from 1.24 K (for pure-U specimen) to 2.11 K (for U-15 at.% Mo). The $H_{c2}(T)$ dependence for the U–Mo alloys determined from the resistivity measurements revealed neither a quadratic dependence nor a linear dependence as the temperature approaches 0 K.

The superconducting transition shows up as a single λ-type peak in the specific heat $C(T)$ for all splats, except for U–Mo11 revealing a double peak feature. The most pronounced λ-type anomaly in the specific heat was found for U–Mo15. The height of the specific heat jump ΔC exceeds the value expected from the BCS theory.

When annealed at 500 °C, the γ-phase in such U–Mo alloys undergoes eutectoid decomposition to form equilibrium phases of orthorhombic α-U and U_2Mo intermetallic (tetragonal γ'-phase), while annealing at 800 °C stabilizes the initial γ phase.

The cubic γ-phase U–Mo15 splat is also very stable in hydrogen atmosphere (no H absorption) below 1 bar and at room temperature. Upon applying high pressure of 80 bar, the powder U–Mo hydride revealing amorphous state was formed. By decomposition U–Mo15 hydride in a vacuum in a closed volume by heating up to 800 °C we could obtain the U–Mo powder (hydrogen was almost entirely released at 500 °C). It points out a new but simple technique for producing the U–Mo powder.

Acknowledgments

This work was supported by Grant Agency of the Czech Republic under the grants numbers P204/10/0330 and P204/12/0285. IT was supported by the Grant Agency of the Charles University under the project no. 675112. Experiments were partly performed at MLTL (http://mltl.eu/), which is supported within the program of Czech Research Infrastructures (project no. LM2011025). N-THK-N expresses her deep thanks to Professor V Sechovsky for his great support for her stay as visiting professor at the Faculty of Mathematics and Physics, Charles University and for the start of this splat-cooling research.

References

[1] Sinha V P, Hegde P V, Prasad G J, Dey G K and Kamath H S 2010 *J. Alloys Compounds* **506** 253 and references therein

[2] Ewh A, Perez E, Keiser D D Jr and Sohn Y H 2010 *J. Phase Equilibria and Diffus.* **31** 216

[3] Meyer M K, Hofman G L, Hayes S L, Clark C R, Wiencek T C, Snelgrove J L, Strain R V and Kim K–H 2002 *J. Nucl. Mater.* **304** 221

[4] Chandrasekhar B S and Hulm J K 1958 *J. Phys. Chem. Solids* **7** 259

[5] Chandrasekhar B S and Bardeen J M 1961 *J. Phys. Chem. Solids* **21** 206

[6] Berlincourt T G 1959 *J. Phys. Chem. Solids* **11** 12

[7] Burke J J, Colling D A, Gorum A E and Greenspan J (ed) 1976 *Physical Metallurgy of Uranium Alloys (Proc. 3rd Army Materials Technology Conf.)* (Vail, CO: Brook Hill)

[8] Brewer L, Lamoreaux R H, Ferro R, Marazza R and Girgis K 1980 *At. Energy Rev.* **7** 336

[9] Hawkins D T and Hultgren R 1973 *Constitution of Binary Alloys* vol 8 8th edn (Metals Park, OH: American Society for Metals)

[10] Hultgren R, Desai P D, Hawkins D T, Gleiser M and Kelley K K 1973 *Selected Values of the Thermodynamic Properties of Binary Alloys* (Metals Park, OH: American Society for Metals)

[11] Lander L H, Fisher E S and Bader S D 1994 *Adv. Phys.* **43** 1

[12] Lashley J C *et al* 2001 *Phys. Rev.* B **63** 224510

[13] Graf D *et al* 2009 *Phys. Rev.* B **80** 24411010

[14] Grenthe I, Drozdzynski J, Fujino T, Buck E C, Albrecht-Schmitt T E and Wolf S F 2006 Uranium *The Chemistry of the Actinide and Transactinide Elements* ed L R Morss, N M Edelstein and J Fuger (New York: Springer) chapter 5

[15] Chiotti P, Klepfer H H and White R W 1959 *Trans. Am. Soc. Met.* **51** 772–82

[16] Van Thyne R J and McPherson D J 1957 *Trans. Am. Soc. Met.* **49** 598

[17] Hofman G L, Meyer M K and Ray A E 1998 Design of high density Gamma-phase uranium alloys for LEU dispersion fuel applications *Proc. Int. Reduced Enrichment for Research and Test Reactors Conf. (18–20 October 1998, Sao Paulo, Brazil)*

[18] Yakel H L 1974 A review of X-ray diffraction studies in uranium alloys *Proc. of the Physical Metallurgy of Uranium Alloys Conf. (12–14 February, 1974, Vail, CO)*

[19] Lehmann Mme J and Hills R F 1960 *J. Nucl. Mater.* **2** 261

[20] Tangri K and Williams G I 1961 *J. Nucl. Mater.* **4** 226

[21] Tkach I, Kim-Ngan N–T H, Mašková S, Dzevenko M, Havela L, Warren A, Stitt C and Scott T 2012 *J. Alloys Compounds* **534** 101

[22] Kim K H, Lee D B, Kim C K, Hofman G E and Paik K W 1997 *J. Nucl. Mater.* **245** 179

[23] Jones H 1973 *Rep. Prog. Phys.* **36** 1425

[24] Ray R and Musso E 1976 Amorphous alloys by splat *US Patent* 3981722

[25] Isserow S 1981 *J. Mater. Sci.* **16** 3214

[26] Poon S J, Drehman A J, Wong K M and Clegg A W 1985 *Phys. Rev.* B **31** 3100

[27] Havela L *et al* 2011 *Intermetallics* **19** 113 and references therein

[28] Parida S C, Dash S, Singh Z, Prasad R and Venugopal V 2001 *J. Phys. Chem. Solids* **62** 585

[29] Hills R F, Howlett B W and Butcher B R 1963 *J. Less-Common Met.* **5** 369

[30] Vatulin A V, Morozov A V, Suprun V B, Petrov Tu I and Trifonov Yu I 2004 *Met. Sci. Heat Treat.* **46** 484

[31] DeLong L E, Huber J G, Yang K N and Maple M B 1983 *Phys. Rev. Lett.* **51** 312

[32] Werthamer N R, Helfand E and Hohenberg P C 1966 *Phys. Rev.* **147** 295

[33] Kolomiets A V, Mašková S, Havela L, Matěj Z and Kužel R 2011 *J. Alloys Compound* **501** 4185